



RESEARCH LETTER

10.1002/2017GL074053

Key Points:

- A manually derived satellite data set of 1735 mesocyclones' trajectories over the Southern Ocean
- The maximum track density was observed over the Bellingshausen Sea and around East Antarctica
- Reanalyses underestimate wind speed in mesocyclones by 25% and consequently the fraction of mesocyclones that are polar lows

Supporting Information:

- Supporting Information S1
- Movie S1

Correspondence to:

P. Verzemskaya,
verzem@sail.msk.ru

Citation:

Verzemskaya, P., N. Tilinina, S. Gulev, I. A. Renfrew, and M. Lazzara (2017), Southern Ocean mesocyclones and polar lows from manually tracked satellite mosaics, *Geophys. Res. Lett.*, *44*, 7985–7993, doi:10.1002/2017GL074053.




Received 4 MAY 2017

Accepted 14 JUL 2017

Accepted article online 19 JUL 2017

Published online 5 AUG 2017

Southern Ocean mesocyclones and polar lows from manually tracked satellite mosaics

Polina Verzemskaya^{1,2} , Natalia Tilinina^{1,3}, Sergey Gulev^{1,4}, Ian A. Renfrew⁵ , and Matthew Lazzara⁶ 

¹P.P. Shirshov Institute of Oceanology, Russian Academy of Sciences, Moscow, Russia, ²Research Computing Center, Moscow State University, Moscow, Russia, ³Alfred Wegener Institute, Helmholtz Centre for Polar and Marine Research, Bremerhaven, Germany, ⁴Research Computing Center, Moscow State University, Moscow, Russia, ⁵School of Environmental Sciences, University of East Anglia, Norwich, UK, ⁶University of Wisconsin-Madison and Madison Area Technical College, Madison, Wisconsin, USA

Abstract A new reference data set of mesocyclone activity over the Southern Ocean has been developed from the manual analysis of high-resolution infrared satellite mosaics for winter 2004. Of the total 1735 mesocyclones which were identified and analyzed, about three quarters were classified as being “polar lows” (i.e., intense systems; see Rasmussen and Turner, 2003). The data set includes mesocyclone track, size, associated cloud vortex type, and background synoptic conditions. Maxima in track density were observed over the Bellingshausen Sea and around East Antarctica and are highly correlated with cyclogenesis regions. A comparison against QuikSCAT and reanalyses wind characteristics shows that the reanalyses, while capturing mesocyclone events, tend to considerably underestimate their wind speed (by up to 10 m s^{-1}). This mesocyclone data set is available as a reference for further analysis of mesocyclones and for the evaluation and development of cyclone-tracking algorithms.

Plain Language Summary Mesocyclones in high latitudes are important maritime atmospheric phenomena, they characterize by strong wind speeds and surface fluxes despite their small sizes (200 to 1000 km) and short lifetime (6 to 36 hours). These characteristics make their identification and tracking difficult in global reanalyses, consequently, they are still poorly documented and quantified, especially, in the Southern Hemisphere. Number of studies demonstrated an overview of mesocyclone activity over the Southern Hemisphere. These studies are based both on automated identification and tracking algorithms and on manual identification and tracking (mostly regional) and show inconsistent assessments. To clarify the Southern Hemisphere mesocyclone activity and to provide a reference dataset, that may be used to validate automated tracking schemes in the Southern Hemisphere we here present manually identified and tracked database of mesocyclones over the Southern Ocean for winter 2004. This database is used to assess the ability of four modern reanalyses to reproduce mesocyclones wind speed field structure in comparison with QuikSCAT scatterometer wind data.

1. Introduction

Mesoscale cyclones (MCs) are high-latitude maritime atmospheric phenomena that are still relatively poorly documented [Rasmussen and Turner, 2003] mostly due to their small size (less than 1000 km in diameter), making their identification and tracking limited in global reanalyses [Condrón *et al.*, 2006; Zappa *et al.*, 2014]. At the same time, MCs, especially polar lows [Rasmussen and Turner, 2003] associated with extreme winds and advection of very dry cold air, play an important role in high-latitude atmospheric dynamics and air-sea interaction processes. Specifically, polar lows are associated with very strong surface air-sea fluxes, triggering intermediate and deep water formation in subpolar latitudes [Condrón *et al.*, 2006; Condrón and Renfrew, 2013]. While the dynamics and structure of individual MCs have been documented for some cases [Watanabe and Niino, 2014; Førre *et al.*, 2012; Wu *et al.*, 2011; Sergeev *et al.*, 2017], climatological assessments are still few especially for the Southern Hemisphere (SH).

Some studies have adapted midlatitude tracking algorithms to select MCs in reanalyses or numerical model outputs [Condrón *et al.*, 2006; Xia *et al.*, 2012; Mallet *et al.*, 2013; Zappa *et al.*, 2014; Laffineur *et al.*, 2014; Watanabe *et al.*, 2016; Yanase *et al.*, 2016]. However, these studies typically underestimate MC activity due to limited spatiotemporal resolution of the reanalyses and lack of assimilated observations, particularly in the SH. As a result, many MCs are either missed or have an underestimated imprint in reanalysis SLP (sea level pressure) and vorticity fields [Condrón *et al.*, 2006].

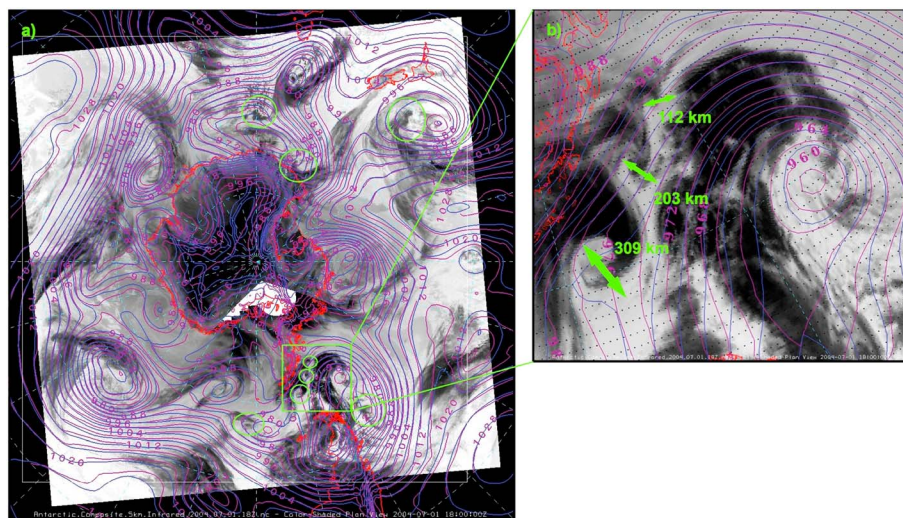


Figure 1. (a) AMRC IR mosaic at 18:00 UTC 7 July 2004 with mesocyclones cloud signatures marked by green circles. (b) Zoom of the region shown by the green rectangle in Figure 1a. Arrows show estimates of cyclone diameters. Black dots in Figure 1b indicate grid points of the NCEP CFSR reanalysis characterized by the highest (among the reanalyses) spatial resolution. Contours are for sea level pressure: ERA-Interim (blue) and MERRA2 (purple).

The use of satellite imagery to derive mesocyclone climatologies can avoid these representation problems but presents other challenges. So far, attempts to manually detect and track polar mesocyclones using cloud signatures from satellite infrared (IR) imagery have been limited to specific regions and relatively short time periods, as the manual procedure is time consuming. For the northeast Atlantic and Nordic Seas, *Harold et al.* [1999a, 1999b] produced a 2 year long satellite-based data set, including more than 4000 MCs—twice as many as identified in ERA-40 reanalysis for the same period [Condrón *et al.*, 2006]. The first climatologies in the SH [Carleton and Carpenter, 1990; Carleton, 1995] were limited by the low frequency (twice daily) of the footprint of satellite data at that time.

We present here a new reference data set developed for the SH using high-resolution IR satellite mosaics covering the winter period of 2004 (June, July, August, and September). By “reference” we refer to potential use of this data set for automated tracking algorithms validation, rather than to the representativeness in terms of climatological conditions.

Section 2 describes the data used and the methods. Section 3 presents MC statistics and provides an assessment of the wind speed fields. It includes a comparison with four modern reanalyses and scatterometer data. Section 4 provides a summary of the results and an outlook. Supporting information provides a detailed description of the manual tracking methodology and statistical information for different types of MCs.

2. Data and Methods

We used 976 satellite infrared (10.3–11.3 μm) mosaics for the winter period of 2004 (June, July, August, and September) available from the Antarctic Meteorological Research Center (AMRC). The winter 2004 was typical in terms of mean sea level pressure variability. Note that the mean 2004 SAM index (for data see <http://www.nerc-bas.ac.uk/icd/gjma/sam.html>) was 0.35 that is twice as small compared to its annual STD (0.69) for the period 1957 to 2017. The mosaics are spatial composites assembling observations from both geostationary and polar orbiting satellites [Lazzara *et al.*, 2003; Kohrs *et al.*, 2014]. The composites cover the squared area encapsulated by the mosaics (Figure 1a) with 5 km spatial and 3-hourly temporal resolution (increased to 4 km and hourly since June 2013). Over ice-covered areas, where it is difficult to accurately distinguish the brightness temperatures of cloud tops and of ice, we also employed water vapor channel ($\sim 6.7 \mu\text{m}$) mosaics, compositing geostationary, and polar orbiting satellite data such as Aqua and Terra via the Moderate Resolution Spectroradiometer (MODIS) [Kohrs *et al.*, 2014]. This water vapor channel has not been used so far for MCs identification but provides useful information over the ice-covered areas [International Workshop on Atmospheric Water Vapor *et al.*, 1980].

Table 1. Number of MCs/Polar Lows With Different Cloud Vortex Types Associated With Different Background Conditions at the Moment of Cyclogenesis

Cloud Vortex Type Synoptic Conditions	Comma	Spiral	Comma-to-Spiral	Merry-Go-Round	Total
Pressure trough	989/711	45/25	104/75	1	1139/811
Center of midlatitude cyclone	160/116	17/15	32/20	0	209/151
Cold-air outbreak	51/45	5/6	5/9	0	61/60
Low-pressure postocclusion zone	90/67	10/9	12/11	14/15	126/102
Orography-induced MCs	31/16	4/2	1	1	37/18
Miscellaneous	147/95	5/2	10/7	1	163/104
Total	1468/1050	86/59	164/122	17/15	1735/1246

The tracking procedure for MCs consists of two steps. First, we manually identified all cloud systems with cyclonic signatures that were less than 1000 km in diameter (Figures 1a and 1b and Movie S1 in the supporting information) and attributed them to polar MCs (Figure 1b). Then, to build the MC trajectories, these systems were manually tracked over their lifetime. Details of the tracking procedure are presented in Text S1. Trajectories were stored for all systems lasting longer than two 3-hourly time steps. For each life cycle time moment, we recorded the following: coordinates of the cyclone center, cyclone diameter (estimated as in Harold *et al.* [1999a]), and associated cloud vortex type (as suggested by Carleton [1995]). Further, we used SLP from ERA-20C [Poli *et al.*, 2015] to identify background synoptic conditions (i.e., synoptic circulation types) at the time moment of cyclogenesis. The choice of ERA-20C was justified by 3-hourly temporal resolution (as in mosaics) and also by its capability to effectively capture background synoptic conditions. The identified background conditions were put into six types (see Table 1); the procedure of classification is described in Text S2. When MCs were paired or clustered (so-called, *cloud trains* or *merry-go-round* [Carleton, 1995]) trajectories of each MC were analyzed separately. The production of the 4 month data set took about 500 h of manual visual analysis and tracking. The data set is available at www.sail.msk.ru/antarctica.

Further, we detected the cloud-determined MCs in four reanalyses products: ERA-Interim [Dee *et al.*, 2011], NCEP CFSR [Saha *et al.*, 2010], JRA55 [Kobayashi *et al.*, 2015], MERRA2 [Bosilovich *et al.*, 2016] as well as in the QuikSCAT SeaWinds data set [Ricciardulli and Wentz, 2015] (see Table S4.1 in Text S4 for the details of these data sets). In these products, we examined scalar wind speed over the MCs' domains (an area exceeding the MC radius by 50 km). To collocate in time 6-hourly reanalyses and 12-hourly QuikSCAT data with 3-hourly satellite tracks derived from mosaics, we used the data snapshots for the closest neighboring time within ± 3 h of the MC occurrence. Note that QuikSCAT data are only available over the ice-free ocean, so only 44% of MC life cycle time moments have been collocated QuikSCAT data.

3. Results

3.1. Mesocyclone Climatology

In total, 1735 MCs were found during June, July, August, and September (JJAS) of 2004 over the SH. The greatest number of MCs was observed in August (556) with 303, 476, and 400 tracks identified in June, July, and September, respectively. All MCs can be categorized into four cloud vortex types: *comma*, *spiral*, *comma-to-spiral*, and *merry-go-round* (Table 1) consistent with Carleton [1995]. Comma forms occur most frequently (84.6% of all cases), with the ratio between "comma" and "spiral" being 11:1, in agreement with Carleton and Carpenter [1990]. For the NH, Harold *et al.* [1999a, 1999b] reported 55% of all MC as comma cloud shape, with many of them being small in size (200–400 km and less). Association of the MC cloud vortex type with a background synoptic situation (following Rasmussen and Turner [2003]; see Table 1) at the onset of cyclogenesis is described with examples in Text S2 in the supporting information [Wilhemssen, 1985; Dannevig, 1954; Fett, 1989; Businger and Reed, 1989; Claud *et al.*, 2009b]. Text S3 shows MC cyclogenesis maps for different background conditions, which define the ability of the atmosphere to maintain or inhibit MC growth and determines the type of the developing system [Uotila *et al.*, 2011; Heinemann and Ebner, 2012; Bracegirdle and Kolstad, 2010; Papritz *et al.*, 2015]. Thus, the most frequent "comma" shape typically occurs in the trough of the midlatitude cyclone (Table 1).

The MC characteristics spatial distribution for JJAS 2004 is illustrated in Figure 2 [Zolina and Gulev, 2002; Tilinina *et al.*, 2013]. We need to note that square shapes of depicted densities are caused by initial

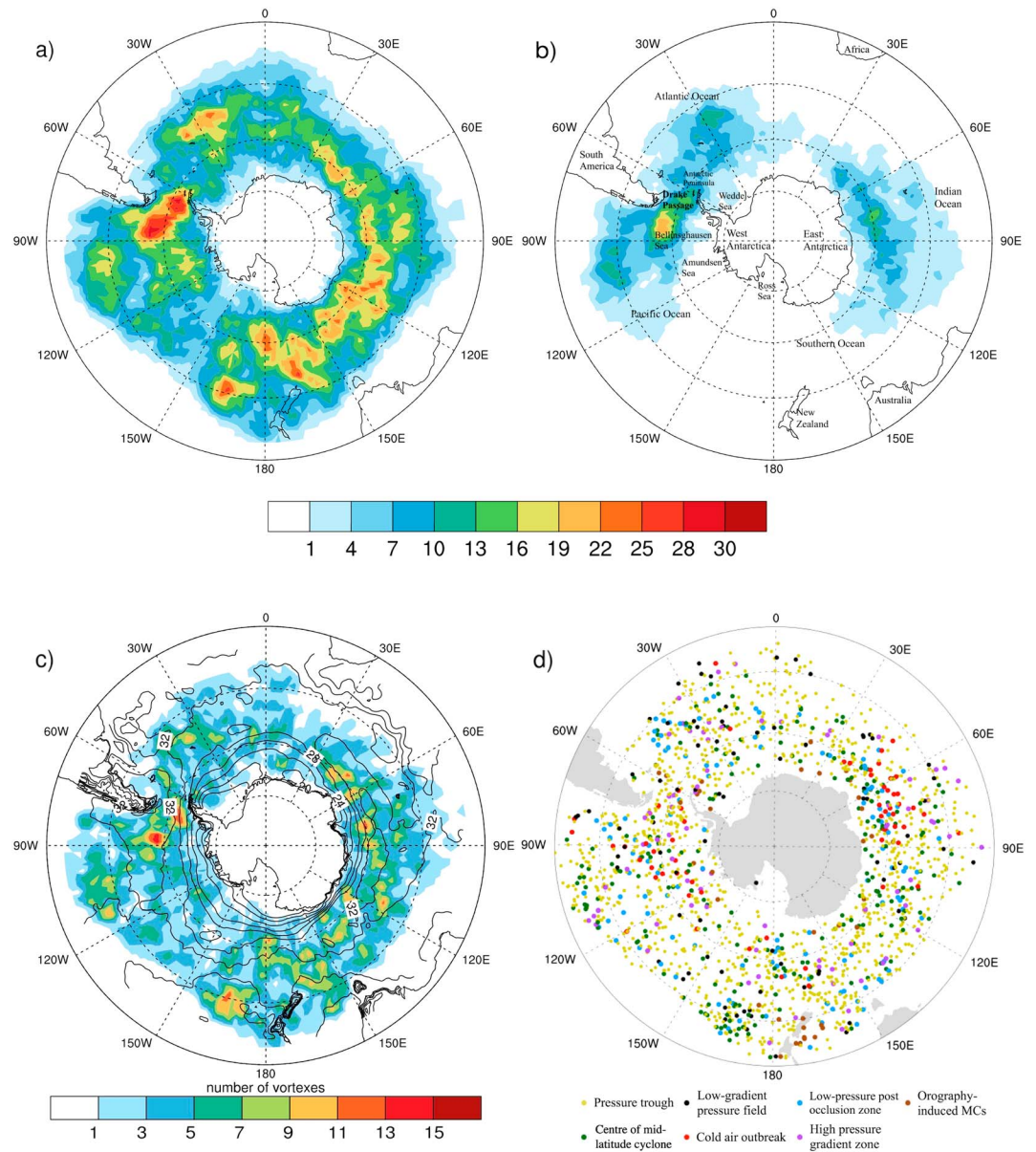


Figure 2. (a) Track densities of all MC for JJAS of 2004, (b) track density for polar lows. (c) MC genesis occurrence superimposed with $\Delta T = T_{surf} - T_{500}$ (black contours), (d) MC genesis events under different background conditions (see colors for definitions of conditions and individual maps in Text S3 in the supporting information). All tracks densities are per 155,000 km².

satellite mosaics square shape, shown on Figure 1. The area covered by the squared mosaics lies south of at least 40°S with the mosaic corners extending to approximately 35°S. In our analysis, we took in to account only the MCs which were generated, developed, and decayed inside the satellite mosaic boundaries. This fully excluded the impact of the so-called entry-exit problem of limited area tracking [see, e.g., Tilinina et al., 2014]. We also estimated the number of MCs whose trajectories were partly captured by the mosaic domain and were not accounted in the analysis. These transients contribute tentatively 3–4% of the total number of MCs and cannot change the major conclusions. Track density (Figure 2a) reveals maxima of MC activity over Drake Passage and eastward of New Zealand (26–30 tracks inside a 2° circle). These maxima are likely associated with the cold air outbreaks (CAOs, see Figure S3.1) that occur in the rear parts of the intense midlatitude systems generated westward of the Antarctic Peninsula and north of Ross Sea [Carrasco et al., 1997a, Carrasco et al., 1997b]. The formation of the latter maximum is closely related to the increase of midlatitude cyclone activity eastward of

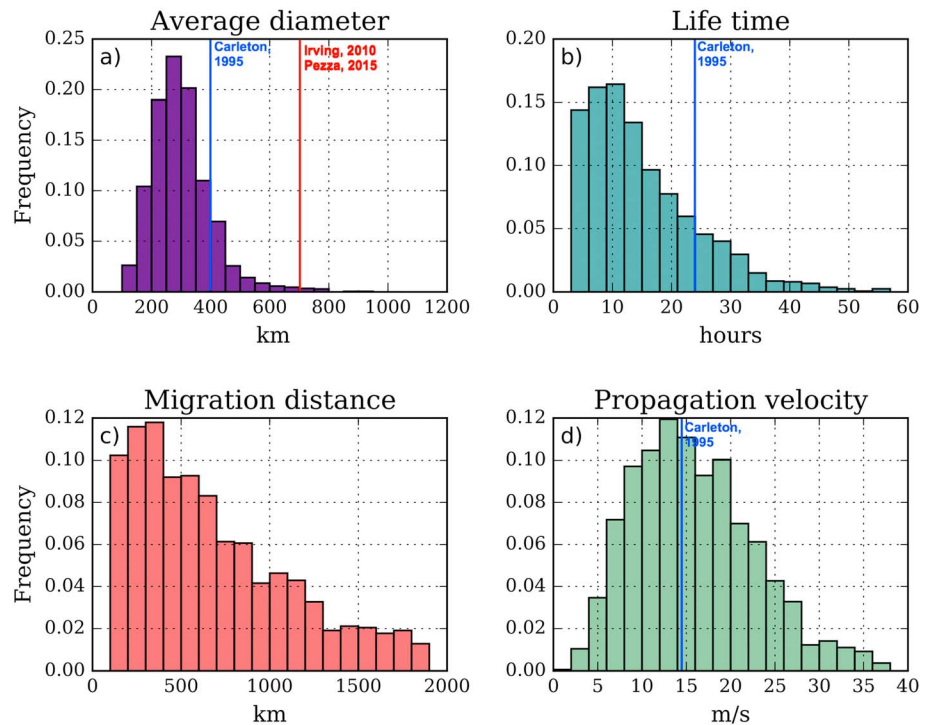


Figure 3. Probability distributions of the life cycle characteristics of MCs. (a) Average diameter (km), (b) lifetime (h), (c) migration distance (km), and (d) propagation velocity (m/s). Bold vertical lines show mean estimates of corresponding parameters reported by previous studies.

New Zealand during winter [Yuan *et al.*, 2009], as most mesocyclones here are associated with the central part of the midlatitude cyclones in the background (see Figure S3.1, types 2 and 4). Another area of intense cyclogenesis along the East Antarctica ice edge (Figure 2c) is associated with CAOs strengthened by katabatic winds (also detectable in Figure S3.1). A maximum in track density over the Bellingshausen Sea and the ice marginal zone of East Antarctica in JJA was reported by Irving *et al.* [2010], although they did not report a pattern eastward of New Zealand. Pezza *et al.* [2016] and Uotila *et al.* [2009] alternatively reported high track densities along coastal East Antarctica; however, they disagreed with each other on the location of the second maximum which was in the Bellingshausen Sea by Pezza *et al.* [2016] and in the Ross Sea by Uotila *et al.* [2009]. The most frequent generation of MCs (Figure 2d) is found in the centers or troughs of midlatitude cyclones (for definitions see Texts S2.1 and S2.2) or in the low-pressure postocclusion zones. About 18.5% of cyclogenesis events in the SH occurred over the Bellingshausen sea and eastward of New Zealand (Figure 2c)—regions characterized by strong vertical atmospheric instability. Typical regions of MC decay are located over the Antarctic Peninsula, Tierra del Fuego, Southern Atlantic islands (24%), and along the East Antarctica ice edge (41% of cyclolysis events, no figure shown).

An analysis of MC life cycle characteristics (Figure 3) shows that their diameters range from 70 km to 1200 km and peak at 300 km which is consistent with Carleton [1995] who reported a mean diameter of 350 km. This is much smaller than estimates derived from reanalyses; for example, Irving *et al.* [2010] and Pezza *et al.* [2016] reported mean diameters of 700 km. The larger sizes of MCs revealed in reanalyses using tracking algorithms are due to an underestimation of the number of relatively small MCs that are not resolved by the coarse spatial resolution products. Irving *et al.* [2010] and Pezza *et al.* [2016] did not account for systems smaller than 400 km, which constitute more than half of our MC sample (Figure 3). Figure 3 shows that the mean MC lifetime is about 12 h (with a maximum of 60 h), the mean migration distance is about 750 km (maximum is 1800 km) and the mean propagation velocity is about 15 m/s (with a maximum of almost 40 m/s). Carleton [1995] reported similar propagation velocities (13–16 m/s) but longer lifetimes (18 to 30 h). This can be explained by many “missed” short-lived MCs in Carleton [1995] due to 12-hourly resolution of satellite data used in his analyses.

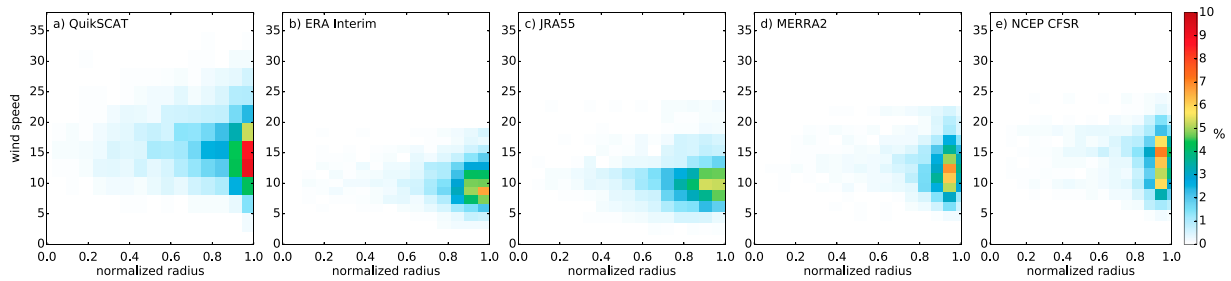


Figure 4. Two-dimensional occurrence diagrams of the maximum wind speed and the location of the maximum relative to the normalized MC radius for (a) QuikSCAT SeaWinds and 4 reanalyses: (b) ERA-Interim, (c) JRA55, (d) MERRA2 and (e) NCEP CFSR. Color scale indicates the percentage of the total number of MCs.

3.2. Evaluation of Mesocyclone Activity in Reanalyses and QuikSCAT Data

While modern high-resolution reanalyses are frequently used for MC studies [Mallet et al., 2013; Laffineur et al., 2014; Zappa et al., 2014], some studies have argued that MCs are too small to be resolved by even high-resolution reanalyses [Condron et al., 2006; Uotila et al., 2009; Zahn and von Storch, 2008; Tilinina et al., 2014]. Here we use our satellite-derived data set to briefly evaluate the ability of modern reanalyses and scatterometers (here QuikSCAT) to capture mesoscale circulations in the SH. We analyze area-averaged and maximum 10 m wind speed over the MC area (defined as the MC radius + 50 km). We also checked areas defined by MC radius + 100 and +150 km, and the results were highly correlated (0.99). Maximum wind speed within the MC was located by its normalized (spanning from 0 to 1) distance R_N from the MC center $R_N = r_p/R_{C50}$, r_p being actual distance and R_{C50} being MC radius plus 50 km. Joint distributions of the maximum wind speed and its normalized distance from the MC center (Figure 4) show that the maximum wind speed is typically detected at the periphery of the MC. About 60% of maximum wind speeds are captured by the 0.8–1.0 range of the nondimensional radius for QuikSCAT; it is 57% and 80% for the JRA55 and NCEP CFSR reanalyses, respectively.

All reanalyses underestimate maximum wind speed magnitudes compared to QuikSCAT: by 5–7 $m s^{-1}$ in ERA-Interim and JRA55, by 3–4 $m s^{-1}$ in MERRA2, and by 1–2 $m s^{-1}$ in NCEP CFSR. The underestimates generally decrease with increasing horizontal resolution.

Q-Q (Quantile-Quantile) plots for the area-averaged and maximum wind speeds show that for the mean wind speed, NCEP CFSR shows the best agreement with QuikSCAT, MERRA2 performs slightly worse, and ERA-Interim and JRA-55 (while consistent with each other) indicate strong negative biases (Figure 5). Underestimation of the wind speed maximum clearly increases with wind speed magnitude in all products. Thus, at the 75th percentile the wind speed is underestimated (compared to QuikSCAT) by 5 $m s^{-1}$ in NCEP CFSR, by 7 $m s^{-1}$ in MERRA2, and by 10 m/s in ERA-Interim and JRA55. The highest recorded wind speed over the MC area in QuikSCAT was 37.9 $m s^{-1}$, while the highest value in reanalyses (MERRA2) was 30 $m s^{-1}$.

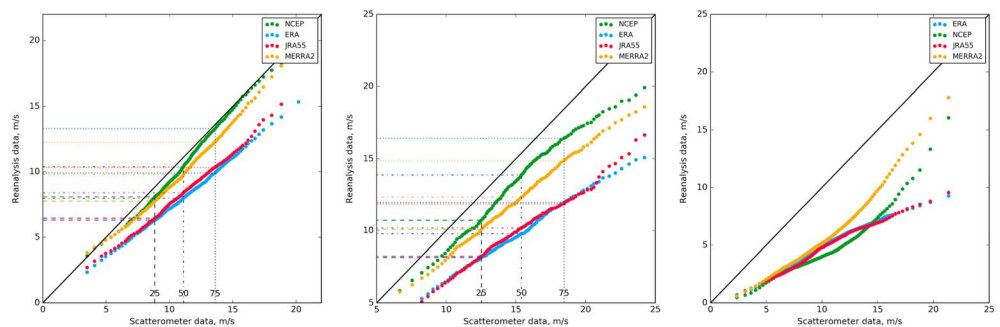


Figure 5. Quantile-quantile plots comparing distributions of the wind speed between QuikSCAT SeaWinds and the four reanalyses. (left) Averaged wind speed over MC area, (middle) maximum wind speed over the MC area, and (right) wind speed over the Southern Ocean south of 40°S. Colors indicate different reanalyses: NCEP CFSR (green), ERA-Interim (blue), JRA55 (red), and MERRA2 (yellow). Dashed lines mark the 25th percentile, dash-dotted line marks the median, and dotted line marks the 75th percentile.

A large underestimation of wind speeds is also evident over the whole Southern Ocean (Figure 5, right); however, over this large area the reanalyses products are comparable for wind speeds up to $\sim 10 \text{ m s}^{-1}$. In this respect, it is important to note that for two products (MERRA2 and NCEP CFSR), underestimation for MCs only is smaller compared to the whole Southern Ocean, which demonstrates the skill of these reanalyses to capture MCs.

We performed a separate analysis for the most intense MCs, polar lows. By using maximum wind speeds from QuikSCAT, we selected vortices that developed over open water and were characterized by maximum wind speeds greater than 15 m/s at least once during their life cycle (herein cyclone life span including generation and decay time moments). These polar lows are primarily located over the Bellingshausen Sea, Drake Passage, and in the southern part of the Indian Ocean (Figure 2b). They are mainly generated west of the Drake Passage and decay typically over Tierra del Fuego. Another polar low storm track aligns with the East Antarctica sea ice marginal zone associated also with the strong low-level baroclinicity and the frequent occurrence of CAOs. A similar distribution for polar lows was reported by *Carleton and Carpenter* [1990] and *Claud et al.* [2009a] for winter season during the El Niño event of 1982, however, they did not report high MC density in the Drake Passage region. In these areas, polar lows contribute 40 to 100% of the total number of MCs. In total 69% of all detected MC tracks can be classified as polar lows, somewhat less than the estimate given in *Irving et al.* [2010]. Similar percentages in reanalyses are much lower being only 14% in ERA-Interim, 20% in JRA 55, 41% in MERRA2, and up to 45% in NCEP CFSR. This is consistent with the underestimation of all wind speed statistics in the reanalyses compared to QuikSCAT (Figure 5). Differences in underestimation can be likely explained by varying spatial resolution [*Jung et al.*, 2006], model physics, and data assimilation schemes in different reanalyses.

4. Conclusions and Outlook

A new satellite-based data set of MCs over the SH for the winter season of 2004 is produced using highly accurate manual tracking applied to the satellite mosaics with 3-hourly temporal and 5 km spatial resolutions. The 1735 MC tracks which we detected were characterized by cloud vortex type, radii, and the associated background synoptic conditions. While the spatial distribution of MC track density is qualitatively consistent with earlier work [*Irving et al.*, 2010; *Lubin et al.*, 2008; *Pezza et al.*, 2016], the number of MCs during winter 2004 is about 2 times larger than in previous studies. Also, life cycle characteristics (e.g., a mean MC diameter of 300 km) are significantly different from the earlier assessments [*Pezza et al.*, 2016; *Irving et al.*, 2010] reporting much larger MCs mean diameters (~ 700 km).

Four modern reanalyses and QuikSCAT SeaWinds data consistently locate wind speed maxima at the periphery of the MCs. Compared to QuikSCAT, all the reanalyses substantially underestimate the absolute maximum of wind speed by 5 to 10 m/s with the higher-resolution NCEP CFSR and MERRA performing much better than ERA-Interim and JRA-55. Polar lows constitute 69% of all detected MCs in QuikSCAT data and much less in the reanalyses (from 14% in ERA-Interim to 45% in NCEP CFSR). Polar lows are mostly located over the East Antarctica coast and the Drake Passage where they contribute between 40 and 100% of the total population of MCs.

Further analysis will include the development and validation of a hybrid algorithm for tracking MCs in high-resolution numerical simulations. This will make it possible to associate characteristics of MCs and polar lows with the deep convection events in the Southern Ocean, first of all, in the Weddell Sea, providing formation of the Antarctic deep water in response to strong diabatic cooling episodes on the surface [*Heinemann*, 1988; *Renfrew et al.*, 2002].

References

- Bosilovich, M. G., R. Lucchesi, and M. Suarez (2016), MERRA-2: File Specification. GMAO Office Note No. 9 (Version 1.1), 73 pp. [Available at http://gmao.gsfc.nasa.gov/pubs/office_notes/]
- Bracegirdle, T. J., and E. W. Kolstad (2010), Climatology and variability of Southern Hemisphere marine cold-air outbreaks, *Tellus Ser. A*, *62*(2), 202–208.
- Businger, S., and R. J. Reed (1989), Cyclogenesis in cold air masses, *Weather Forecasting*, *2*, 110–133.
- Carleton, A. M. (1995), On the interpretation and classification of mesoscale cyclones from satellite infrared imagery, *Int. J. Remote Sens.*, *16*(13), 2457–2485.
- Carleton, A. M., and D. A. Carpenter (1990), Satellite climatology of ‘polar lows’ and broadscale climatic associations for the Southern Hemisphere, *Int. J. Climatol.*, *10*(3), 219–246.

Acknowledgments

This work was supported by the SCAR early career scientists fellowship. We thank Dan Pollak, Bradley Yehl, and Andrew Carleton from Penn State who provided us with nondigitized maps of mesocyclones’ manual tracks for the same period. We appreciate editorial comments from Linda Keller, the help of Denis Sergeev in the development of tracking software. This work was supported by the Russian Science Foundation grant 17-77-20112 (P.V. and N.T., analysis of storm tracks) and by the contract with Russian Ministry of Education and Science 14.W03.31.0006 (S.K.G., analysis of satellite data). Also, support was provided by the Russian Foundation for Basic Research grant 14-05-00969. I.R. was supported in part by NE/J005703/1. Materials from M.L. are based upon the work supported by the United States NSF under grants PLR-1141908 and PLR-1244924. The data set is available at www.sail.msk.ru/antarctica.

- Carrasco, J. F., D. H. Bromwich, and Z. Liu (1997a), Mesoscale cyclone activity over Antarctica during 1991: 1. Mary Bird Land, *J. Geophys. Res.*, *102*, 13,923–13,937, doi:10.1029/97JD00905.
- Carrasco, J. F., D. H. Bromwich, and Z. Liu (1997b), Mesoscale cyclone activity over Antarctica during 1991: 2. Near the Antarctic Peninsula, *J. Geophys. Res.*, *102*, 13,939–13,954, doi:10.1029/97JD00904.
- Claud, C., A. M. Carleton, B. Duchiron, and P. Terray (2009a), Atmospheric and upper ocean environments of Southern Ocean polar mesocyclones in the transition season months and associations with teleconnections, *J. Geophys. Res.*, *114*, D23104, doi:10.1029/2009JD011995.
- Claud, C., A. M. Carleton, B. Duchiron, and P. Terray (2009b), Southern hemisphere winter cold-air mesocyclones: Climatic environments and associations with teleconnections, *Clim. Dyn.*, *33*, 383–408, doi:10.1007/s00382-008-0468-5.
- Condron, A., and I. A. Renfrew (2013), The impact of polar mesoscale storms on northeast Atlantic Ocean circulation, *Nat. Geosci.*, *6*(1), 34–37.
- Condron, A., G. R. Bigg, and I. A. Renfrew (2006), Polar mesoscale cyclones in the northeast Atlantic: Comparing climatologies from ERA-40 and satellite imagery, *Mon. Weather Rev.*, *134*(5), 1518–1533.
- Dannevig, P. (1954) *Meteorologi for Flygere [in Norwegian]*, Ashehoug, Oslo.
- Dee, D. P., et al. (2011), The ERA-Interim reanalysis: Configuration and performance of the data assimilation system, *Q. J. R. Meteorol. Soc.*, *137*(656), 553–597.
- Fett, R. W. (1989), Polar low development associated with boundary layer fronts in the Greenland, Norwegian and Barents seas, in *Polar and Arctic Lows*, edited by P. F. Twitchell, E. Rasmussen, and K. L. Davidson, pp. 313–322, A Deepak, Hampton, Va.
- Føre, I., J. E. Kristjansson, E. W. Kolstad, T. J. Bracegirdle, Ø. Saetra, and B. Røsting (2012), A 'hurricane-like' polar low fuelled by sensible heat flux: High-resolution numerical simulations, *Q. J. R. Meteorol. Soc.*, *138*, 1308–1324, doi:10.1002/qj.1876.
- Harold, J. M., G. R. Bigg, and J. Turner (1999a), Mesocyclone activity over the north-East Atlantic. Part 1: Vortex distribution and variability, *Int. J. Climatol.*, *19*(11), 1187–1204.
- Harold, J. M., G. R. Bigg, and J. Turner (1999b), Mesocyclone activity over the Northeast Atlantic. Part 2: An investigation of causal mechanisms, *Int. J. Climatol.*, *19*(12), 1283–1299.
- Heinemann, G. (1988), On the structure and energy budget of the boundary layer in the vicinity of the Filchner/Ronne ice shelf front (Antarctica), *Beitr. Phys. Atmos.*, *61*, 244–258.
- Heinemann, G., and L. Ebner (2012), *Cyclone and Mesocyclone Tracking in the Antarctic Region and Southern Polar Ocean*, European Polar Low Working Group Workshop, Oslo, Norway.
- International Workshop on Atmospheric Water Vapor, A. Deepak, L. H. Ruhnke, T. D. Wilkerson, and United States (1980), *Atmospheric water vapor*, edited by A. Deepak, T. D. Wilkerson, and L. H. Ruhnke, Academic Press, New York.
- Irving, D., I. Simmonds, and K. Keay (2010), Mesoscale cyclone activity over the ice-free Southern Ocean: 1999–2008, *J. Clim.*, *23*(20), 5404–5420.
- Jung, T., S. K. Gulev, I. Rudeva, and V. Soloviev (2006), Sensitivity of extratropical cyclones characteristics to horizontal resolution in the ECMWF model, *Q. J. R. Meteorol. Soc.*, *132*, 1839–1857, doi:10.1256/qj.05.212.
- Kobayashi, S., et al. (2015), The JRA-55 reanalysis: General specifications and basic characteristics, *J. Meteorol. Soc. Atmos.*, *93*(1), 5–48.
- Kohrs, R. A., M. A. Lazzara, J. O. Robaidek, D. A. Santek, and S. L. Knuth (2014), Global satellite composites – 20 years of evolution, *Atmos. Res.*, *135–136*, 8–34, doi:10.1016/j.atmosres.2013.07.023.
- Laffineur, T., C. Claud, J. P. Chaboureaud, and G. Noer (2014), Polar lows over the Nordic Seas: Improved representation in ERA-Interim compared to ERA-40 and the impact on downscaled simulations, *Mon. Weather Rev.*, *142*(6), 2271–2289.
- Lazzara, M. A., L. M. Keller, C. R. Stearns, J. E. Thom, and G. A. Weidner (2003), Antarctic satellite meteorology: Applications for weather forecasting, *Mon. Weather Rev.*, *131*, 371–383.
- Lubin, D., R. A. Wittenmyer, D. H. Bromwich, G. J. Marshall, and G. J. (2008), Antarctic Peninsula mesoscale cyclone variability and climatic impacts influenced by the SAM, *Geophys. Res. Lett.*, *35*, L02808, doi:10.1029/2007GL032170.
- Mallet, P. E., C. Claud, C. Cassou, G. Noer, and K. Kodera (2013), Polar lows over the Nordic and Labrador Seas: Synoptic circulation patterns and associations with North Atlantic-Europe wintertime weather regimes, *J. Geophys. Res. Atmos.*, *118*, 2455–2472, doi:10.1002/jgrd.50246.
- Papritz, L., S. Pfahl, H. Sodemann, and H. Wernli (2015), A climatology of cold air outbreaks and their impact on air–sea heat fluxes in the high-latitude South Pacific, *J. Clim.*, *28*(1), 342–364.
- Pezza, A., K. Sadler, P. Uotila, T. Vihma, M. D. Mesquita, and P. Reid (2016), Southern Hemisphere strong polar mesoscale cyclones in high-resolution datasets, *Clim. Dyn.*, *47*(5–6), 1647–1660.
- Poli, P., H. Hersbach, P. Berrisford, D. Dee, A. Simmons and P. Laloyaux (2015), ERA-20C deterministic, *ERA Rep. Ser.*, *20*.
- Rasmussen, E. A., and J. Turner (2003), *Polar Lows: Mesoscale Weather Systems in the Polar Regions*, 612 pp., Cambridge Univ. Press, Cambridge.
- Renfrew, I. A., J. C. King, and T. Markus (2002), Coastal polynyas in the southern Weddell Sea: Variability of the surface energy budget, *J. Geophys. Res.*, *107*(C6), 3063, doi:10.1029/2000JC000720.
- Ricciardulli, L., and F. J. Wentz (2015), A scatterometer geophysical model function for climate-quality winds: QuikSCAT Ku-2011, *J. Atmos. Ocean. Technol.*, *32*(10), 1829–1846.
- Saha, S., et al. (2010), The NCEP climate forecast system reanalysis, *Bull. Am. Meteorol. Soc.*, *91*(8), 1015.
- Sergeev, D. E., I. A. Renfrew, T. Spengler and S. R. Dorling (2017), Structure of a shear-line polar low, *Q. J. R. Meteorol. Soc.*, *143*, 12–26, doi:10.1002/qj.2911.
- Tilina, N., S. K. Gulev, I. Rudeva, and K. P. Koltermann (2013), Comparing cyclone life cycle characteristics and their interannual variability in different reanalyses, *J. Clim.*, *26*, 6419–6438, doi:10.1175/JCLI-D-12-00777.1.
- Tilina, N., S. K. Gulev, and D. Bromwich (2014), New view of Arctic cyclone activity from the Arctic system reanalysis, *Geophys. Res. Lett.*, *41*, 1766–1772, doi:10.1002/2013GL058924.
- Uotila, P., A. B. Pezza, J. J. Cassano, K. Keay, and A. H. Lynch (2009), A comparison of low pressure system statistics derived from a high-resolution NWP output and three reanalysis products over the Southern Ocean, *J. Geophys. Res.*, *114*, D17105, doi:10.1029/2008JD011583.
- Uotila, P., T. Vihma, A. B. Pezza, I. Simmonds, K. Keay, and A. H. Lynch (2011), Relationships between Antarctic cyclones and surface conditions as derived from high-resolution numerical weather prediction data, *J. Geophys. Res.*, *116*, D07109, doi:10.1029/2010JD015358.
- Watanabe, S. I., and H. Niino (2014), Genesis and Development Mechanisms of a Polar Mesocyclone over the Japan Sea, *Mon. Weather Rev.*, *142*, 2248–2270, doi:10.1175/MWR-D-13-00226.1.
- Watanabe, S. I., H. Niino, and W. Yanase (2016), Climatology of polar mesocyclones over the sea of Japan using a new objective tracking method, *Mon. Weather Rev.*, *144*, 2503–2515, doi:10.1175/MWR-D-15-0349.1.
- Wu, L., J. E. Martin, and G. W. Petty (2011), Piecewise potential vorticity diagnosis of the development of a polar low over the Sea of Japan, *Tellus A*, *63*, 198–211.

- Wilhemsen, K. (1985), Climatological study of gale-producing polar lows near Norway, *Tellus A*, 37A, 451–459, doi:10.1111/j.1600-0870.1985.tb00443.x.
- Xia, L., M. Zahn, K. I. Hodges, and F. Feser (2012), A comparison of two identification and tracking methods for polar lows, *Tellus A*, 64, doi:10.3402/tellusa.v64i0.17196.
- Yanase, W., H. Niino, S. I. I. Watanabe, K. I. Hodges, M. Zahn, T. Spengler, and I. A. Gurvich (2016), Climatology of polar lows over the sea of Japan using the JRA-55 reanalysis, *J. Clim.*, 29(2), 419–437.
- Yuan, X., J. Patoux, and C. Li (2009), Satellite-based midlatitude cyclone statistics over the Southern Ocean: 2. Tracks and surface fluxes, *J. Geophys. Res.*, 114, D04106, doi:10.1029/2008JD010874.
- Zahn, M., and H. von Storch (2008), A long-term climatology of North Atlantic polar lows, *Geophys. Res. Lett.*, 35, L22702, doi:10.1029/2008GL035769.
- Zappa, G., L. Shaffrey, and K. I. Hodges (2014), Can polar lows be objectively identified and tracked in the ECMWF operational analysis and the ERA-Interim reanalysis?, *Mon. Weather Rev.*, 142(8), 2596–2608.
- Zolina, O., and S. K. Gulev (2002), Improving accuracy of mapping cyclone numbers and frequencies, *Mon. Weather Rev.*, 130, 748–759.